Three- and two-photon absorption spectroscopy: REMPI of HCl and HBr

Ágúst Kvaran, Huasheng Wang, and Benedikt G. Waage

Abstract: Approximation expressions for absorption line strengths due to $\Omega' = 0, 1, 2, 3 \leftarrow \Omega'' = 0$ (Σ, Π, Δ, and $\Phi \leftarrow \Sigma$) transitions for three-, two-, and one-photon absorptions are summarized. Those for three- and two-photon absorptions are used to analyse room temperature $(3 + 1)$ and $(2 + 1)$ REMPI (resonance enhanced multiphoton ionization) spectra due to transitions to Rydberg states in HCl and HBr to give spectroscopic parameters. A mechanism of the three-photon excitation process for the $(E^1\Sigma^+) \leftarrow X(^1\Sigma^+)$, $(0, 0)$ transition in HCl is proposed. A Rydberg state, not observed in single- or two-photon absorption, with a band origin at 80 167 cm^{-1} was identified in $(3 + 1)$ REMPI of HBr and analysed for the first time. It was assigned to the $l(^3\Phi(\Omega' = 3))$ $((\sigma^2\pi^3)5d\delta)$ state, $(0, 0)$ band. Use of the three-photon absorption line strength expressions for deriving rotational population distributions in ground-state HBr is demonstrated.

PACS Nos.: 03.40Kf, 42.65Tg, 42.81Dp

Résumé : Nous résumons les expressions approximatives pour l'intensité des lignes d'absorption dans les transitions $\Omega' = 0, 1, 2, 3 \leftarrow \Omega'' = 0$ (Σ, Π, Δ et $\Phi \leftarrow \Sigma$) par l'absorption de 1, 2 ou 3 photons. Les cas à deux et trois photons sont utilisés pour obtenir les paramètres spectroscopiques à partir des spectres REMPI « resonance enhanced multiphoton ionization » $(2 + 1)$ et $(3 + 1)$ à température de la pièce résultant de transitions vers des états de Rydberg dans HCl et HBr. Nous proposons un mécanisme pour l'excitation à trois photons $(E^1\Sigma^+) \leftarrow X(^1\Sigma^+)$, (0, 0) dans HCl. Nous avons identifié et analysé pour la première fois par REMPI $(3 + 1)$ dans HBr un état de Rydberg dont l'origine de bande est à 80 167 cm^{-1} et qui est inobservable par absorption de un ou deux photons. Nous lui avons assigné l'état $l(^3\Phi(\Omega' = 3))$ $((\sigma^2\pi^3)5d\delta)$, bande $(0, 0)$. Nous montrons comment utiliser les expressions pour l'intensité des lignes d'absorption à trois photons afin d'obtenir les distributions de population rotationnelle dans le fondamental de HBr.

[Traduit par la Rédaction]

1. Introduction

Advantages of using multiphoton absorption methods in spectroscopy are associated with (*i*) increasing the number of allowed transitions as the number af absorbing photons increases and (*ii*) the use of lower energy photons for accessing higher energy states.

Only a rather limited number of high-resolution spectroscopy work involving three-photon absorption has been performed. This work has mainly been done by using the REMPI (resonance enhanced

Received July 1, 2000. Accepted November 26, 2000. Published on the NRC Research Press Web site on May 3, 2001.

Á. Kvaran,[1] H. Wang, and B.G. Waage. Science Institute, University of Iceland, Dunhaga 3, 107 Reykjavík, Iceland.

[1] Corresponding author (e-mail: agust@raunvis.hi.is). Home page: http://www.raunvis.hi.is/~agust.

 DOI: 10.1139/cjp-79-2/3-197

multiphoton ionization) technique for small gas-phase molecules such as H_2 [1], O_2 [2], CO_2 [3,4], CS_2 [5–7], Cl_2 [8], and HBr [9]. Both single- and two-photon absorption spectra studies of diatomic molecules largely make use of Hönl–London-type expressions for line intensities [10,11]. Analogous expressions for three-photon absorptions have only recently been presented and used [9]. Hönl–London-type expressions were derived for the transitions strengths of $\Omega' = 0, 1, 2$ and $3 \leftarrow \Omega'' = 0$ (alternatively, Σ, Π, Δ, and $\Phi \leftarrow \Sigma$) three-photon transitions from more general expressions given by Halpern et al. [12]. These have been shown to be useful for assigning states observed in $(3 + 1)$ REMPI and to simulate spectra due to three-photon excitations to $\Omega' = 0(\Sigma)$, $1(\Pi)$, and $3(\Phi)$ states in HBr [9].

In addition to using REMPI spectra for deriving information about the characteristics of the states involved, their use to derive information about populations in quantum states in reaction dynamics has proved to be useful [13–15]. In this context care must be given to the effects of possible perturbations, due to state interactions, that may affect line positions and intensities. This is a well-known phenomenon in the hydrogen halides where both homogenenous and heterogeneous interactions have been observed [16,17]. Due to the nature of the multiphoton absorption, the effects of intermediate and virtual states on the excitation process also needs to be considered. Recently, this has been dealt with for two-photon excitations in the hydrogen halides [16,17]. No absorbing bound electronic states are found in a large part of the lower energy region of the neutral hydrogen halide molecules [18–20]. The lowest energy bound states reported are the $b_2\ ^3\Pi_2$ states, for which $T_e = 76\,322$ and $67\,663$ cm^{-1} for HCl ($IP = 102\,820$ cm^{-1}) and HBr ($IP = 94\,125$ cm^{-1}), respectively [20]. This minimizes the effect of intermediate states on the structure of the multiphoton absorption spectra.

In this paper, we demonstrate the use of the Hönl–London approximation expressions for identifying and simulating the $(E^1\Sigma^+) \leftarrow X(^1\Sigma^+)$ $(0, 0)$ spectrum for HCl and two $\Omega' = 2$ (Δ) states for HBr in $(3 + 1)$ REMPI spectra. A comparison is made between these spectra and the $(2 + 1)$ REMPI corresponding ones. Furthermore, we report the first observation of an $\Omega' = 3$ HBr Rydberg state, which has not been observed in either single- or two-photon absorption. A comparison of calculated and measured rotational line intensities for the $i(^3\Delta_2) \leftarrow X(^1\Sigma^+)$ transition in HBr shows that the approximation expressions are useful for deriving rotational level populations.

2. Experimental

The experimental setup was similar to that described in refs. 21–23. Tunable UV laser pulses were generated by a Lumonics Hyperdye 300 laser pumped by XeCl/308 nm laser pulses from a Lumonics 510 excimer laser. The bandwidth of the laser beam was about 0.05 cm^{-1}. The wavelength range 349–388 nm was covered by using the dyes TMQ (349–362 nm), BPBD (361–387 nm), and BBQ (375–388 nm). The laser pulses were reflected 90° by a Pellin Broca prism and focused midway between two stainless steel electrodes (15 mm diameter and about 20 mm apart) inside a simple glass ionization cell. The electrodes were typically kept at ±250 V. Gas sample pressure in the region, 0.5–5 Torr (1 Torr = 133.3 Pa), was chosen by maximizing the signal due to ionization. Gas samples from lecture bottles (Merck, HCl: 99.5%; HBr: 99.8%) were thoroughly degassed by a series of freeze, pump, and thaw cycles and transfered to the ionization cell at room temperature (20°C). Voltage drop pulses from the electrodes, following laser ionization, were amplified by a balanced bias differential amplifier [24], integrated by an integration circuit. Typically 100 pulses (20 Hz laser repetition rate; 5 s sampling time) were sampled and averaged by a LeCroy 9310 A, 400 MHz storage oscilloscope and fed into a computer for spectra displaying and manipulations (software: Test Point, Capital Equipment Corporation). The dye laser output was scanned in 0.05–0.2 cm^{-1} steps for recording spectra. Care was taken to prevent power-broadening by minimizing laser power. Calibration of the wavelength was achieved by recording the REMPI of chlorine and bromine atomic lines [9,17]. The accuracy of the calibration was found to be about ±2 cm^{-1} on the two- and three-photon wave-number scales. Spectra intensities were corrected for possible intensity drift during the scan. Furthermore, the effect of varying laser power was corrected

for by dividing the measured intensity by the power cubed for the (3 + 1) REMPI spectra and by the power squared for the (2 + 1) REMPI spectra.

3. Spectra structure and calculations

Transition strengths for electronic transitions in diatomic molecules ($S(n, \Omega', J)$) have been formulated in terms of Hönl–London-type approximation expressions for one- [10], two- [11], and three-photon [9] absorptions. The transition strengths are the sum and product functions of the Hönl–London factors (s_i) and transition moment functions μ_i^2 as listed in Table 1 for various electronic transitions from $\Omega'' = 0\,(\Sigma)$. The $s_i's$ ($i = 0, 1, 2, 3$) are functions that depend on the electronic angular momentum projection quantum number, Ω' and on the total angular momentum quantum numbers J' and J'' (i.e., s_i (Ω', J, ΔJ); $J = J''$ and $\Delta J = J' - J''$). The μ_i^2 functions are the sum and product functions of all one-photon transition moments and energy denominators that give rise to parallel ($\mu_{||}$) and perpendicular ($\mu_{\pm}$) transitions [9,11,12]. The primed and unprimed notations for the single photon transition moments ($\mu = \mu_{||}$ or $\mu_{\pm}$) in Table 1 refer to transitions

(1) one photon absorption: $|1> \overset{\mu}{\leftarrow} |0>$

(2) two photon absorption: $|1> \overset{\mu}{\leftarrow} |i> \overset{\mu'}{\leftarrow} |0>$

(3) three photon absorption: $|1> \overset{\mu}{\leftarrow} |i2> \overset{\mu'}{\leftarrow} |i1> \overset{\mu''}{\leftarrow} |0>$

where $|1>$ and $|0>$ are the resonance excited state and the ground state, respectively. $|i>$, $|i2>$, and $|i1>$ are virtual intermediate states. The μ_i^2 functions depend on the number of absorbed photons (n) and Ω' (i.e., $\mu_i^2\,(n, \Omega')$) [11,12]. The subscript numbers ($i = 0$–3) refer to orders of Clebsch–Gordan coefficients in terms of which these expressions can be written [9,12]. The general selection rules in terms of the electron angular momentum projection quantum numbers $\Delta\Omega\,(= \Omega' - \Omega'')$ can be derived directly from Table 1.

$$\Delta\Omega = 0,\ \pm 1, \ldots\ \pm n; \qquad n = 1, 2, 3, \ldots$$

By inspection of the J-dependent s_i expressions [9–11], general selection rules in terms of the total angular momentum quantum numbers also can be determined.

$$\Delta J = 0, \pm 1, \ldots \pm n; \quad n = 1, 2, 3, \ldots; \qquad \Delta\Omega > 0$$

$$\Delta J = \pm 1, \ldots \pm n; \quad n = \text{odd numbers}; \qquad \Delta\Omega = 0$$

$$\Delta J = 0, \pm 2, \ldots \pm n; \quad n = \text{even numbers}; \qquad \Delta\Omega = 0$$

Although the $\mu_i^2\,(n, \Omega')$ functions can, in principle, be measured from spectra, more commonly these are treated as unknown variables in comparisons of spectra line intensities and transition strengths [9,13,16,17]. Thus, in analysis of rotational structure the *signal intensity* (I_{rel}) can be expressed as

$$I_{\text{rel}} = \{C_i s_i(\Omega', J) + C_j s_j(\Omega', J)\} \exp\left(\frac{-E(J)}{kT}\right) \tag{1a}$$

for those transitions where the transition strengths are expressed by *two* terms (i.e., $S(2, 0, J)$, $S(3, 0, J)$, and $S(3, 1, J)$; see Table 1) and as

$$I_{\text{rel}} = C s_i(\Omega', J) \exp\left(\frac{-E(J)}{kT}\right) \tag{1b}$$

Table 1. (*a*) Forms of absorption transition strengths ($S(n, \Omega', J) = \Sigma\mu_i^2(n, \Omega')s_i(\Omega', \Delta J)$) for n ($n = 1, 2, 3$) number of photons absorbed for $\Omega' \leftarrow \Omega'' = 0$ ($\Omega' = 0, 1, 2, 3$) transitions ($J = J''$ and $\Delta J = J' - J''$) and (*b*) expressions for μ_i^2 functions (see text).

	$\Omega' = 0$ (Σ)	$\Omega' = 1$ (Π)	$\Omega' = 2$ (Δ)	$\Omega' = 3$ (Φ)
(a)				
$S(1, \Omega', J)$ *	$\mu_1^2(1, 0)s_1(0, J)$	$\mu_1^2(1, 1)s_1(1, J)$	0	0
$S(2, \Omega', J)$ †	$\mu_0^2(2, 0)s_0(0, J)$ $+ \mu_2^2(2, 0)s_2(0, J)$	$\mu_2^2(2, 1)s_2(1, J)$	$\mu_2^2(2, 2)s_2(2, J)$	0
$S(3, \Omega', J)$ ‡	$\mu_1^2(3, 0)s_1(0, J)$ $+ \mu_3^2(3, 0)s_3(0, J)$	$\mu_1^2(3, 1)s_1(1, J)$ $+ \mu_3^2(3, 1)s_3(1, J)$	$\mu_3^2(3, 2)s_3(2, J)$	$\mu_3^2(3, 3)s_3(3, J)$
(b)				
$\mu_1^2(1, \Omega')$ *	$(\mu_{\|\|})^2$	$(\mu_+)^2$	—	—
$\mu_0^2(2, \Omega')$ †	$(\mu_{\|\|}\mu'_{\|\|} + \mu_-\mu'_+)^2$	—	—	—
$\mu_2^2(2, \Omega')$ †	$(2\mu_{\|\|}\mu'_{\|\|} - \mu_-\mu'_+)^2$	$(\mu_+\mu'_{\|\|} + \mu_{\|\|}\mu'_+)^2$	$(\mu_+\mu'_+)^2$	—
$\mu_1^2(3, \Omega')$‡	$(\mu_{\|\|}\mu'_{\|\|}\mu''_{\|\|} + 1/5(2\mu_-\mu'_+\mu''_{\|\|}$ $-3\mu_-\mu'_{\|\|}\mu''_+ - 3\mu_{\|\|}\mu'_-\mu''_+$ $+4\mu_{\|\|}\mu'_{\|\|}\mu''_{\|\|}))^2$	$(\mu_+\mu'_-\mu''_+ + \mu_-\mu'_+\mu''_+ - \mu_{\|\|}\mu'_{\|\|}\mu''_+$ $+1/5(\mu_+\mu'_-\mu''_+ + \mu_-\mu'_+\mu''_+$ $+2\mu_{\|\|}\mu'_{\|\|}\mu''_+ - 3\mu_{\|\|}\mu'_+\mu''_{\|\|}$ $-3\mu_+\mu'_{\|\|}\mu''_{\|\|}))^2$	—	—
$\mu_3^2(3, \Omega')$ ‡	$(\mu_-\mu'_+\mu''_{\|\|} + \mu_-\mu'_{\|\|}\mu''_+$ $+\mu_{\|\|}\mu'_-\mu''_+ + 2\mu_{\|\|}\mu'_{\|\|}\mu''_{\|\|})^2$	$(\mu_+\mu'_-\mu''_+ + \mu_-\mu'_+\mu''_+ + 2\mu_{\|\|}\mu'_{\|\|}\mu''_+$ $+2\mu_{\|\|}\mu'_+\mu''_{\|\|} + 2\mu_+\mu'_{\|\|}\mu''_{\|\|})^2$	$(\mu_+\mu'_+\mu''_{\|\|} + \mu_+\mu'_{\|\|}\mu''_+$ $+\mu_{\|\|}\mu'_+\mu''_+)^2$	$(\mu_+\mu'_+\mu''_+)^2$

* See ref. 10, p. 208.

† See ref. 11, tables 2 and 3 and ref. 12, pp. 8 and 9.

‡ See refs. 9 and 12, p. 14.

Table 2. Band origins (ν^o) and rotational parameters (B and D) for HCl and HBr states. Excited state parameters were derived from simulations of (3 + 1) REMPI and (2 + 1) REMPI spectra for the E, i, and I states, but from (3 + 1) REMPI spectrum for the l state.

				ν^o		B (cm $^{-1}$)		$D \times 10^{-3}$ (cm^{-1})		Ref.
State:	Configs.	Ion core	ν'	Ours'	Others'	Ours'	Others'	Ours'	Others'	Others'
HCl										
$X(^1\Sigma^+)$	$\sigma^2\pi^4$	—	0	—	—	—	10.439 826	—	0.508 771 23	20
$(E^1\Sigma^+)$	$(\sigma^2\pi^3)5p\pi$	$^2\Pi_{1/2}$	0	83 781±2	83 780.0	6.615±0.040	6.6257	3.8±0.5	3.113 4	18
HBr										
$X(^1\Sigma^+)$	$\sigma^2\pi^4$	—	0	—	—	—	8.348 244	—	0.331 6574	20
$i^3\Delta(2)$ [a]	$(\sigma^2\pi^3)5d\pi$	$^2\Pi_{3/2}$	0	78 625±2	78 630.7	7.975±0.030 (e)	7.968 (e)	0.55±0.10 (e)	0.5 (e)	19
						7.969±0.030 (f)	7.981 (f)	0.50±0.10 (f)	0.6 (f)	
$l^3\Phi(3)$ [a]	$(\sigma^2\pi^3)5d\delta$	$^2\Pi_{3/2}$	0	80 167±3	—	8.38±0.04(e)	—	0.87±0.10(e)	—	—
						8.38±0.04(f)		0.75±0.10(f)		
$I^1\Delta(2)$ [a]	$(\sigma^2\pi^3)5d\pi$	$^2\Pi_{1/2}$	0	81 311.03±2	81 311.5	7.920±0.030 (e)	7.958 (e)	0.51±0.10 (e)	1.1 (e)	19
						7.901±0.030 (f)	7.792 (f)	0.30±0.10 (f)	–1.5 (f)	

[a] Energies of rotational levels with parity $+(-1)^J$ (e levels; O, Q, and S lines) and with parity $-(-1)^J$ (f levels; N, P, R, and T lines) are expressed as $E(J) = B_v{}^i\ J(J+1) - D_v{}^i\ J^2(J+1)^2$, where $B_v{}^i$ and $D_v{}^i$ are effective rotational constants (see p. 228 of ref. 10 and ref. 18).

Fig. 1. Calculated rotational line series (N, P, R, and T) for three-photon absorption, relevant to (3 + 1) REMPI spectra of HCl due to the $\Omega' = 0 \leftarrow \Omega'' = 0$ ($\Sigma \leftarrow \Sigma$) transitions. Rotational constants used are $B'' = 10.439\,826\ \mathrm{cm}^{-1}$, $D'' = 0.508\,771\,23 \times 10^{-3}\ \mathrm{cm}^{-1}$ (= $B_{v''=0}$ and $D_{v''=0}$ for the ground state, $X(^1\Sigma^+)$; see Table 2), $B' = 6.62\ \mathrm{cm}^{-1}$ and $D' = 0.0038\ \mathrm{cm}^{-1}$. Boltzmann distribution for $T = 298$ K is assumed. Spectra contributions are plotted against relative three-photon wave-number scale. μ_1^2:μ_3^2 = 0:1 (top), (1:1) (middle), and (1:0) (bottom).

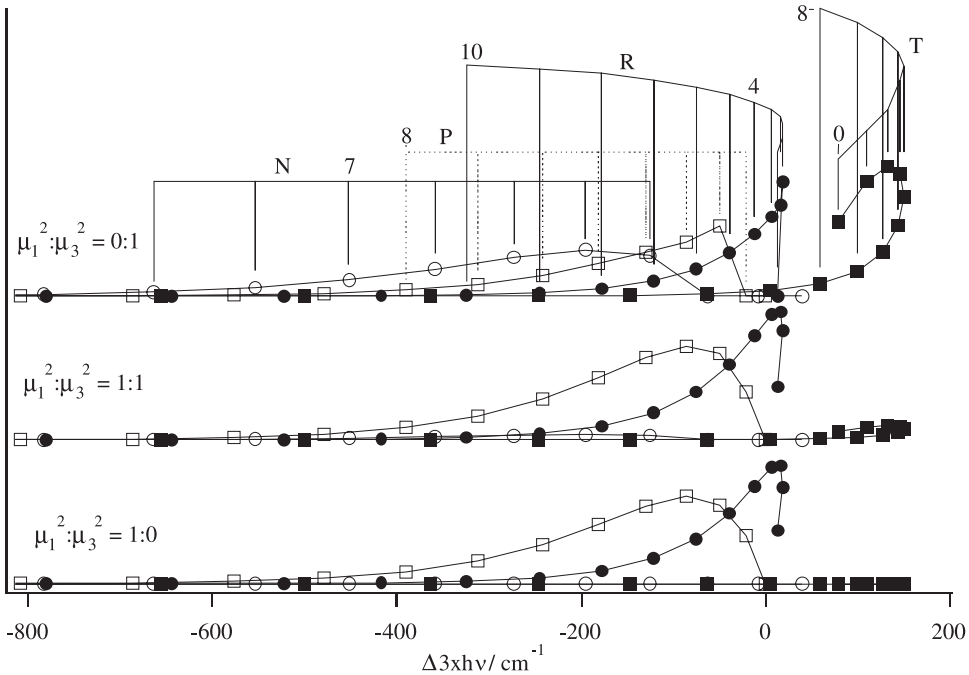

for those transitions where the transition strengths are expressed by a *single* term (see Table 1). In the former case, $\mu_i^2/\mu_j^2 = C_i/C_j$. Evaluated μ_i^2/μ_j^2 ratios obtained from (2 + 1) REMPI spectra have been interpreted, to predict the effect of intermediate/virtual states on two-photon excitation processes [16,17,25] for $\Omega' = 0 \leftarrow \Omega'' = 0(\Sigma \leftarrow \Sigma)$ transitions based on the expressions for μ_0^2 (2, 0) and μ_2^2 (2, 0) (see Table 1).

Signal line positions for rovibrational lines $\left(\nu_{J',v' \leftarrow J'',v''}\ \mathrm{cm}^{-1}\right)$ can be expressed as

$$\nu_{J',v' \leftarrow J'',v''} = \nu^{\mathrm{o}}_{v',v''} + \Delta \bar{E}_{J',J''} \tag{2}$$

where $\nu^{\mathrm{o}}_{v',v''}$ is the band origin (in cm^{-1}) of a vibrational band. $\Delta \bar{E}_{J',J''}$ is the difference in rotational energies (in cm^{-1}), depending on the rotational parameters (B', D', B'', and D'') and the rotational quantum numbers (J', J'') [9,16].

Figure 1 shows examples of calculated rotational contributions of rovibrational bands relevant to three-photon excitations to a $\Omega' = 0$ Rydberg state in HCl (see below), for which the line intensities are μ_1^2 (3, 0) and μ_3^2 (3,0) dependent, see (1a). Line series for $\mu_1^2(3, 0) = 0$, $\mu_3^2(3, 0) \neq 0$ (top), $\mu_1^2(3, 0) = \mu_3^2(3, 0)$ (middle), and $\mu_1^2(3, 0) \neq 0$, $\mu_3^2(3, 0) = 0$ (bottom) are shown. The following characteristics of the three-photon absorption spectra for $\Omega' = 0 \leftarrow \Omega'' = 0$ can be derived from these calculated spectra, Table 1, and the above mentioned selection rules:

- No O, Q, and S rotational lines are observed.
- The spectrum for $\mu_3^2(3, 0) = 0$ is identical to the single-photon absorption spectrum, showing P and R rotational line series only.

Fig. 2. HCl ($H^{35}Cl$; $H^{37}Cl$), $(E^1\Sigma^+) \leftarrow X(^1\Sigma^+)$, (0, 0) room temperature (20°C) REMPI spectra analysis: (*a*) Comparison of (2+1) REMPI (above) and (3+1) REMPI (below) experimental spectra. J'' numbers and rotational lines for $H^{35}Cl$ are indicated. Isotope splitting shows in the (2+1) REMPI spectrum as indicated. Unassigned peaks in the (2 + 1) REMPI spectrum are due to the $V(^1\Sigma^+) \leftarrow X(^1\Sigma^+)$ ($v' = 10$ and 11) transitions. (*b*) Simulation of the (3 + 1) REMPI spectrum. Experimental spectrum (top), calculated rotational line contributions (bottom) and simulated spectrum (underneath the experimental spectrum).

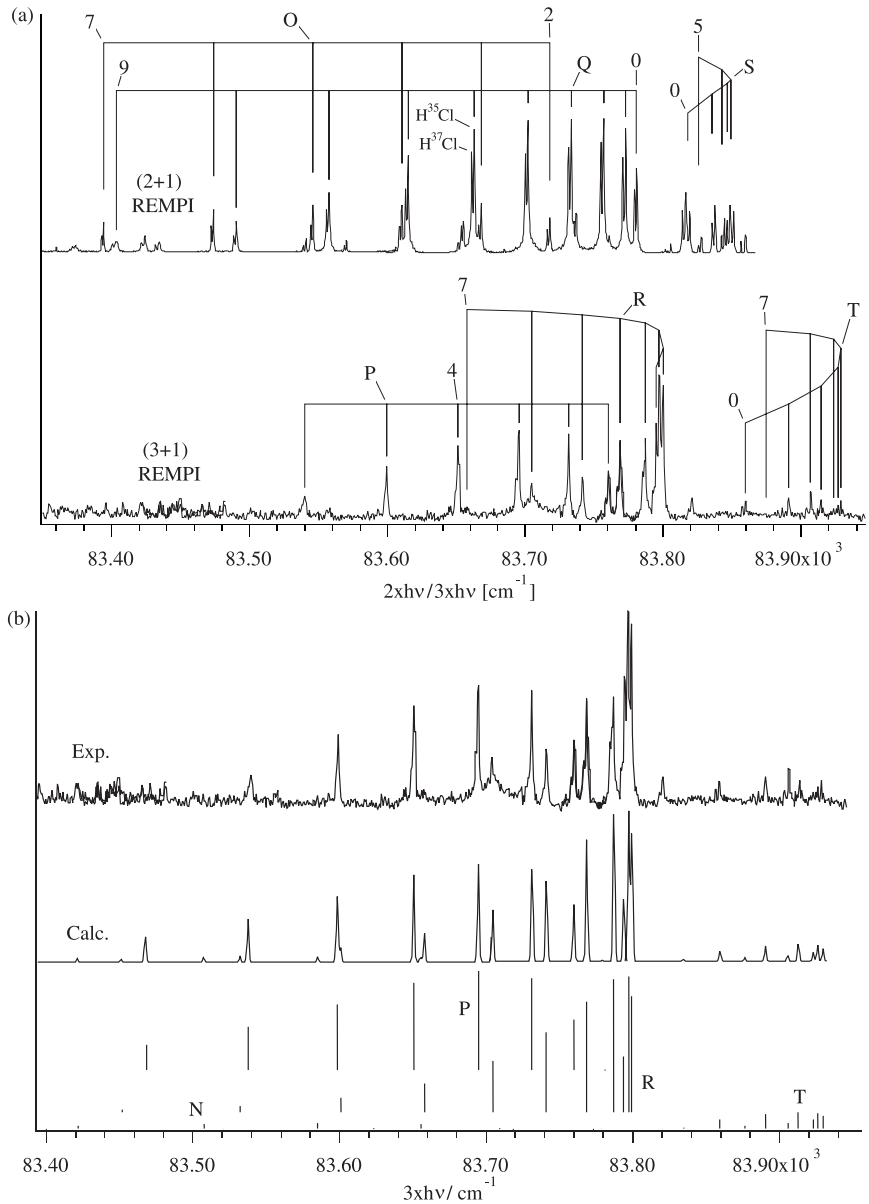

- The intensities of the N and the T line series increase relative to those of the P and R line series as the ratio $\mu_1^2(3,0)$ / $\mu_3^2(3,0)$ decreases.
- The relative intensities of the first rotational lines in the P and the R line series ($J'' = 1$ and 0, respectively) drop as $\mu_1^2(3,0)/\mu_3^2(3,0)$ decreases and equal zero for $\mu_1^2(3,0) = 0$.

Table 3. Transition moment functions (μ_1^2 and μ_3^2) and ratios ($\mu_1^2\ (3,0)/\mu_3^2\ (3,0)$) for the four major channels (see text) in $\Omega' = 0 \leftarrow \Omega'' = 0(\Sigma \leftarrow \Sigma)$ three-photon absorption.

Chan.	St. |1>	St. |i2>	St. |i1>	St. |0>	$\mu_1^2(3,0)$	$\mu_3^2(3,0)$	$\frac{\mu_1^2(3,0)}{\mu_3^2(3,0)}$
1	Σ	Σ	Σ	Σ	$(81/25)\{\mu_{\|\|}\mu'_{\|\|}\mu''_{\|\|}\}^2$	$4\{\mu_{\|\|}\mu'_{\|\|}\mu''_{\|\|}\}^2$	0.81
2	Σ	Π	Σ	Σ	$(4/25)\ \{\mu_{-}\mu'_{+}\mu''_{\|\|}\}^2$	$1\ \{\mu_{-}\mu'_{+}\mu''_{\|\|}\}^2$	0.16
3	Σ	Σ	Π	Σ	$(9/25)\ \{\mu_{\|\|}\mu'_{-}\mu''_{+}\}^2$	$1\ \{\mu_{\|\|}\mu'_{-}\mu''_{+}\}^2$	0.36
4	Σ	Π	Π	Σ	$(9/25)\ \{\mu_{-}\mu'_{\|\|}\mu''_{+}\}^2$	$1\ \{\mu_{-}\mu'_{\|\|}\mu''_{+}\}^2$	0.36

Calculated (simulated) spectra for three-photon excitations to $\Omega' = 2$ and 3 Rydberg states (in HBr) will be dealt with in more detail in the next chapter.

4. Results and analysis

4.1. HCl: $E(^1\Sigma^+) \leftarrow X(^1\Sigma^+)$, (0, 0)

Figure 2*a* shows (2 + 1) REMPI (top) and (3 + 1) REMPI (below) spectra in the excitation region 83 300–83 940 cm^{-1}. The main features of the spectra can be assigned to the $(E^1\Sigma^+) \leftarrow X(^1\Sigma^+)$, (0, 0) system, which has been seen before, both in single-photon absorption [26,27] and in (2 + 1) REMPI [18,28]. The (2 + 1) REMPI spectrum also shows rotational lines due to the $V(^1\Sigma^+) \leftarrow X(^1\Sigma^+)$ ($v' = 10$ and 11) systems. The $(E^1\Sigma^+) \leftarrow X(^1\Sigma^+)$ spectra show clear rotational line series: (*i*) O, Q, and S branches in (2 + 1) REMPI and (*ii*) P, R, and T branches in (3 + 1) REMPI. These observations are in agreement with expectations. Observed and absent rotational line series follow the selection rules given above. At the bottom of Fig. 2*b* are shown calculated rotational line contributions to the (3 + 1) REMPI spectrum obtained by using the calculation procedure described above. A simulated spectrum is shown directly underneath the experimental spectrum in Fig. 2*b*.

Simultaneous simulations of the (2 + 1) and (3 + 1) REMPI spectra revealed the spectroscopic parameters listed in Table 2 along with values obtained by others. The rotational constants were determined with a rather large uncertainty. This is due to the fact that the $(E^1\Sigma^+)$ state is heavily perturbed by homogeneous interaction with the $V(^1\Sigma^+)$ ion-pair state making the standard expression for the rotational energy levels ($E(J)$) in terms of two rotational constants (B' and D')

$$E(J') = B'J'(J'+1) - D'J'^2(J'+1)^2 \tag{3}$$

not fully satisfactory. The determination of the spectroscopic parameters is solely based on the comparison of the *positions* of calculated and experimental rotational lines, but independent of line intensities. The simulation procedure was carried out by a least-squares analysis technique for the line positions.

The relative intensities of the rotational lines in both spectra are determined by (1a). The parameters C_i and C_j were adjusted to obtain the best visible fits of *line intensities* and to determine the $\mu_0^2(2,0)/\mu_2^2(2,0)$ and the $\mu_1^2(3,0)/\mu_3^2(3,0)$ ratios for the two- and the three-photon absorption spectra, respectively (see above). Thus, $\mu_0^2(2,0)/\mu_2^2(2,0) \sim 0.25$ has been reported before [16] and $\mu_1^2(3,0)/\mu_3^2(3,0) = 0.90 \pm 0.15$ was obtained. It has been argued that the value $\mu_0^2(2,0)/\mu_2^2(2,0) \sim 0.25$ for two-photon absorption could be a cause of a dominant two-parallel-transitions excitation mechanism [16]. In the case of a three-photon excitation, four major excitation channels are involved:

$$(1)\Sigma(|1>) \overset{\mu_{\|}}{\leftarrow} \Sigma(|i2>) \overset{\mu'_{\|}}{\leftarrow} \Sigma(|i1>) \overset{\mu''_{\|}}{\leftarrow} \Sigma(|0>)$$

$$(2)\Sigma(|1>) \overset{\mu_{-}}{\leftarrow} \Pi(|i2>) \overset{\mu'_{+}}{\leftarrow} \Sigma(|i1>) \overset{\mu''_{\|}}{\leftarrow} \Sigma(|0>)$$

$$(3)\Sigma(|1>) \overset{\mu_{\|}}{\leftarrow} \Sigma(|i2>) \overset{\mu'_{-}}{\leftarrow} \Pi(|i1>) \overset{\mu''_{+}}{\leftarrow} \Sigma(|0>)$$

$$(4)\Sigma(|1>) \overset{\mu_{-}}{\leftarrow} \Pi(|i2>) \overset{\mu'_{\|}}{\leftarrow} \Pi(|i1>) \overset{\mu''_{+}}{\leftarrow} \Sigma(|0>)$$

Fig. 3. HBr, i($^3\Delta(2)$) $\leftarrow^1\Sigma^+$), (0, 0) room temperature (20°C) REMPI spectra analysis: (*a*) Comparison of (2+1) REMPI (above) and (3 + 1) REMPI (below) experimental spectra. J'' numbers and rotational lines are indicated. Q-branch lines due to the V($^1\Sigma^+$) $\leftarrow$ X($^1\Sigma^+$) ($v' = m + n$ ($n = 10, 11$), $v'' = 0$) systems overlap in the regions below 81 200 cm^{-1} ($n = 10$) and above 81 600 cm^{-1} ($n = 11$) in the (2 + 1) REMPI spectrum. (*b*) Simulation of the (3 + 1) REMPI spectrum. Experimental spectrum (top), calculated rotational line contributions (bottom) and simulated spectrum (underneath the experimental spectrum).

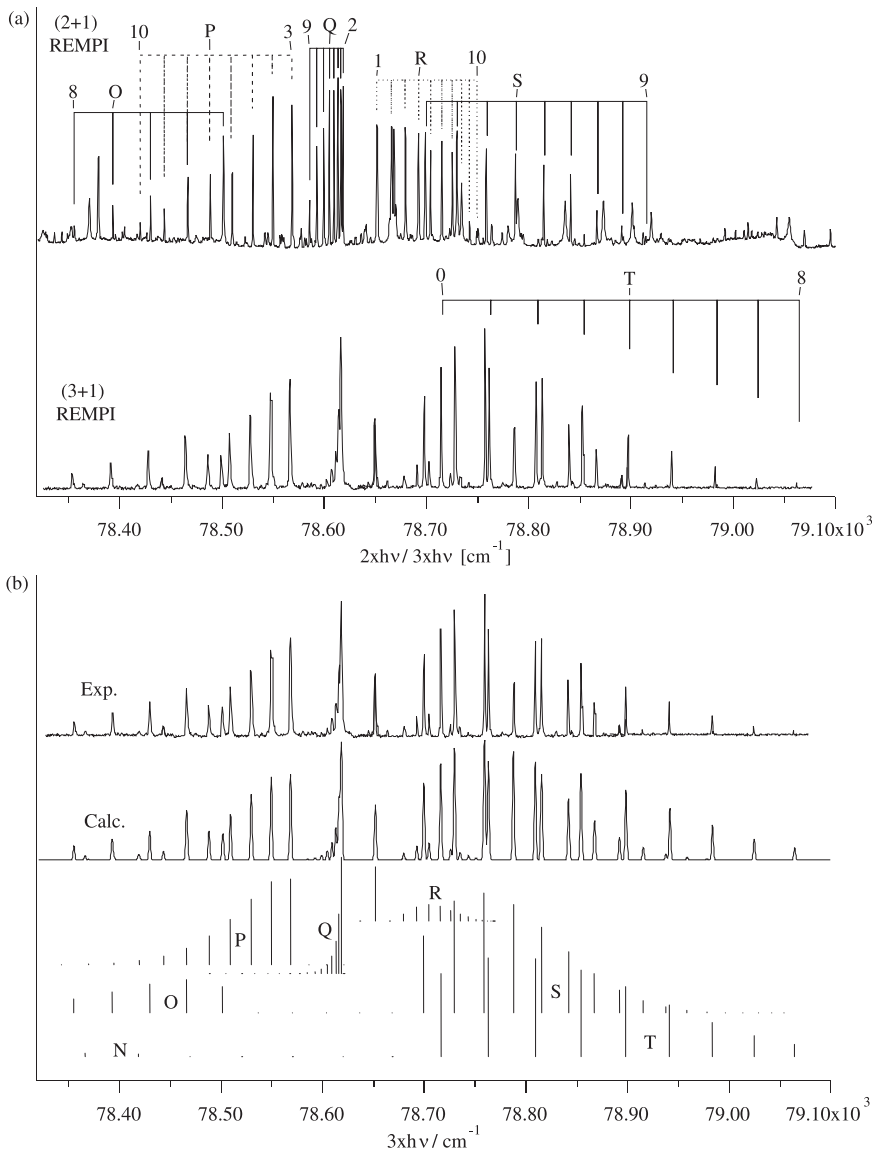

Relevant expressions for $\mu_1^2(3, 0)$ and $\mu_3^2(3, 0)$ as well as values for $\mu_1^2(3, 0)/\mu_3^2(3, 0)$ ratios evaluated from Table 1 are to be found in Table 3. Judging from the weight factors (numbers) in the expressions for $\mu_1^2(3, 0)$ and $\mu_3^2(3, 0)$ (Table 3: 81/25 and 4 for channel 1, respectively) and comparison of observed (0.90 ± 0.15) and predicted (0.81 for channel 1) $\mu_1^2(3, 0)/\mu_3^2(3, 0)$ ratios, there is a reason to believe that a three-parallel-transition's (channel 1) excitation mechanism is dominating in the E ($^1\Sigma^+$) $\leftarrow$ X($^1\Sigma^+$),

(0, 0) three-photon transition. This could be symbolized by

$$E([\sigma^2\pi^3]5p\pi) \leftarrow \{i2[\sigma^2\pi^3]\pi\} \leftarrow \{i1[\sigma^2\pi^3]\pi\} \leftarrow X([\sigma^2\pi^4])$$

where $[\sigma^2\pi^3]\pi$ represent all virtual Rydberg states with π Rydberg electron configurations.

4.2. HBr: $\Omega' = 2(\Delta) \leftarrow X(^1\Sigma^+)$, (0, 0)

Figure 3*a* shows (2 + 1) REMPI (top) and (3 + 1) REMPI (below) spectra in the excitation region 78 300–79 100 cm^{-1} for HBr. The main features of the spectra can be assigned to the $i(^3\Delta_2) \leftarrow X(^1\Sigma^+)$, ($v' = 0$, $v'' = 0$) system, which has been seen before in (2 + 1) REMPI [19]. The main features of the (2 + 1) and (3 + 1) REMPI spectra in the excitation region 81 000–81 700 cm^{-1} can be assigned to the $I(^1\Delta_2) \leftarrow X(^1\Sigma^+)$, ($v' = 0$, $v'' = 0$) system, which also has been seen before in (2 + 1) REMPI [19]. Q-branch lines due to the $V(^1\Sigma^+) \leftarrow X(^1\Sigma^+)$ ($v' = m+10$, $v'' = 0$), and ($v' = m+11$, $v'' = 0$) systems overlap in the regions below 81 200 cm^{-1} and above 81 600 cm^{-1}, respectively, in the (2 + 1) REMPI spectrum. All these spectra show N, O, P, Q, R, S, and T lines as expected (see above). At the bottom of Fig. 3*b* are shown calculated rotational line contributions to the $i(^3\Delta_2) \leftarrow X(^1\Sigma^+)$, (0, 0)/(3 + 1) REMPI spectrum obtained by using the calculation procedure described above. A simulated spectrum is shown directly underneath the experimental spectrum in Fig. 3*b*.

The relative intensities of the rotational lines in the (3 + 1) REMPI spectra were determined by (1b). Comparison of the calculated and the experimental spectra reveals the following characteristics of a spectrum due to an $\Omega' = 2 \leftarrow \Omega'' = 0$ transition at room temperature:

- The Q line intensities gradually decrease with increasing quantum number from $J_{min} = 2$.
- The $J = 1$ rotational lines in the R branch characteristically stick out as a relatively strong peak, but the $J = 2$ line is absent.
- The $J = 0$ rotational line in the S series is not seen.

Simulations of both the (2 + 1) and the (3 + 1) REMPI spectra revealed the spectroscopic parameters listed in Table 2 along with values obtained by others. The rotational constants derived for the $I(^1\Delta_2)$ state differ significantly from those obtained by Green et al. from jet-cooled samples using conventional analysis methods [18]. We believe that the larger number of rotational lines in our spectra (20°C; both (2 + 1) and (3 + 1) REMPI) as well as the simulation analysis technique makes our values more reliable.

4.3. HBr: $l^3\Phi(3) \leftarrow X(^1\Sigma^+)$, (0, 0)

Figure 4 shows the (3 + 1) REMPI spectrum in the excitation region 80 000–80 400 cm^{-1}. The spectrum clearly displays the main characteristics to be expected for a three-photon absorption spectrum due to a $\Omega' = 3 \leftarrow \Omega'' = 0$ transition [9]:

- The N, O, and P lines are much weaker than the R, S, and T lines while the Q lines are of medium strength.
- A characteristic large gap is observed between the Q-branch lines and the first rotational lines on both sides of it (in the P and R line series)
- A gradual decrease in rotational lines of the S and T series is observed as J increases (for room temperature).

Furthermore the Q-branch peak is particularly sharp, suggesting that the rotational constant for the upper state closely resembles the one for the ground state. Simulated spectrum and calculated rotational contributions are shown on Fig. 4. A few unidentified peaks are found on the long-wave-number side of

Fig. 4. HBr, l($^3\Phi$(3)) ←X($^1\Sigma^+$), (0, 0) room temperature (20°C) REMPI spectra simulation: Experimental spectrum (top), calculated rotational line contributions (bottom) and simulated spectrum (underneath the experimental spectrum).

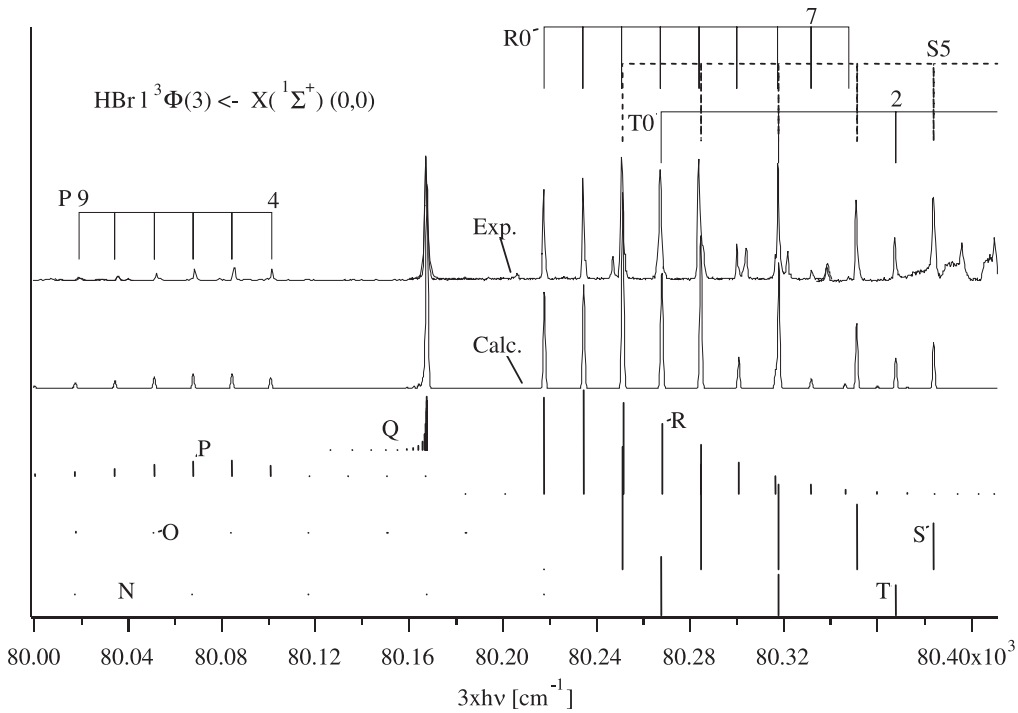

the Q-branch lines. Notice that rotational lines overlap in a characteristic way, so that peaks in the S-line series overlap every other peak in the R branch and peaks in the T-line series overlap every third peak in the R branch. This affects the intensity alteration of peaks as predicted in the simulation. Spectroscopic parameters derived from the simulation are listed in Table 2.

The upper state for this system ($\nu^o = 80\,167$ cm^{-1}) has not been observed and assigned before. We assign it to the l($^3\Phi_3$(3)) ($v' = 0$) state based on the following. Two of four Rydberg states belonging to the dδ manifold (($\sigma^2\pi^3$)5dδ) and converging to the $^2\Pi_{3/2}$ spin–orbit component of the ground ionic state (X($^2\Pi_\Omega$)) have been reported in this spectral area, i.e., the k($^3\Pi_0$(0)) ($\nu^o = 80\,036.9$ cm^{-1}) and the k($^3\Pi_1$(1)) ($\nu^o = 80\,386.0$ cm^{-1}) states [29]. The remaining states that belong to this category and which are expected to be found in this region are the l($^3\Phi_3$(3)) and the l($^3\Phi_4$(4)) states. The $\Omega' = 3$, singlet state (L($^1\Phi_3$(3))), which also belongs to the dδ manifold but converges to the $^2\Pi_{1/2}$ spin–orbit component of the ionic state, has been observed at $\nu^0 = 82\,837$ cm^{-1} , i.e., about 2670 cm^{-1} higher in energy. Other states that belong to this same category are close in energy (k($^3\Pi_2$(2)) ($\nu^o = 82\,676.9$ cm^{-1}) [29], K($^1\Pi$(1)) ($\nu^o = 83\,453$ cm^{-1}) [19,29] and l($^3\Phi_2$(2)) ($\nu^o = 82\,583$ cm^{-1}) [19]). The separation (2670 cm^{-1}) can be compared with the spin–orbit splitting, 2651.4 cm^{-1} , for the ground-state ion [20]. Transitions to triplet states in single- and two-photon absorption are generally found to be important in the hydrogen halides, suggesting that spin–orbit coupling is significant in these molecules.

An alternative assignment for the $\nu^o = 82\,837$ cm^{-1} band (L($^1\Phi_3$(3)), $v' = 0$ state [9]) is the l($^3\Phi_3$(3)) ($v' = 1$) state, in which case the vibrational spacing between $v' = 0$ and 1 (2670 cm^{-1}) is comparable with that for the ground state (2558.54 cm^{-1} [20]). This might be expected for states with comparable rotational constants ($B' = 8.38$ cm^{-1}, $B'' = 8.348\,244$ cm^{-1} ; see Table 2), hence

comparable average internuclear distances. Close similarity of states, however, suggests unfavorable Franck–Condon overlap for the $v' = 1$ and $v'' = 0$ wave functions, hence low transition probability (or) weak spectral intensity, opposite of what is found. We, therefore, believe that our observation of the $l(^3\Phi_3(3))$ $(v' = 0)$ state further strengthens our previous assignment of the $\nu^o = 82\,837\ \text{cm}^{-1}$ band [9].

4.4. Population distribution

The Hönl–London expressions for three-photon absorptions are derived by assuming that for the approximations (*i*) all intermediate virtual states, taking part in the excitation process, are largely off-resonance and (*ii*) that those of the same symmetry are replaced by a single representative state. Therefore, care must be taken with the effects of these approximations on the predicted line intensities in the calculations. We tested the validity of the Hönl–London factors for obtaining rotational populations in the absorbing state $(P(J);\ J = J'')$ from the (3 + 1) REMPI, HBr ($i(^3\Delta_2) \leftarrow X(^1\Sigma^+)$, (0,0)) spectrum. That particular spectrum was chosen because of limited overlap of spectral peaks in a technically convenient spectral region (near the 380 nm photon wavelength).

We assumed that the intensity of the rotational lines $(I(J))$ could be expressed as

$$I(J) = CS(3, \Omega', J)\left\{\frac{P(J)}{(2J+1)}\right\} \tag{4}$$

where C is a constant and $S(3, \Omega', J)$ is the transition strength for three-photon absorption (see above). In the case of a thermal (Boltzmann) distribution $(P(J) \sim (2J+1)\exp(-E(J)/kT))$ this expression can be written as

$$I(J) = CS(3, \Omega', J)\exp\left(\frac{-E(J)}{kT}\right) \tag{5a}$$

giving

$$\ln\left(\frac{I(J)}{S(3, \Omega', J)}\right) = -\left(\frac{1}{kT}\right)E(J) + \ln C \tag{5b}$$

Therefore, a plot of the logarithm of the ratio of the measured line intensities $(I(J))$ over the relevant Hönl–London factor $(S(3, \Omega', J))$ as a function of the rotational level energies in the ground state $(E(J))$ should give straight lines with slope $(-1/kT)$. Figure 5 shows such plots for the various rotational line series in the (3 + 1) REMPI spectrum of HBr due to the transition $i(^3\Delta_2) \leftarrow X(^1\Sigma^+)$, (0, 0) (Fig. 3). Plots for individual rotational line series were normalized to fit straight lines with zero intersect values ($\ln C = 0$; $C = 1$). The continuous straight line is a best line fit through all the data points (all line series O, .. T) with $\ln C = 0$ and $(-1/kT) = -0.0055$ cm. The broken line is a straight line corresponding to a thermal distribution for 20°C/room temperature, $\ln C = 0$ and $(-1/kT) = -0.0049$ cm. This shows that the rotational population can indeed be predicted by (4) within experimental error.

5. Conclusions

Easy to use, Hönl–London-type expressions for transition strengths of three-photon absorptions due to transitions from $\Omega'' = 0$ (Σ) for diatomic molecules are summarized along with analogous expressions for two- and one-photon absorptions. General forms of absorption intensities for one-, two- and three-photon absorptions, based on the Hönl–London factors and transition moment functions, are presented. The approximation expressions are used to demonstrate what spectra structures are expected to be seen in $\Omega' = 0 \leftarrow \Omega'' = 0$ $(\Sigma \leftarrow \Sigma)$ three-photon absorptions. (2 + 1) and (3 + 1) REMPI spectra due to transitions to the Rydberg states ($E^1\Sigma^+$ $(\Omega' = 0)$) in HCl and the $i(^3\Delta(\Omega' = 2))$ and $I(^1\Delta(\Omega' = 2))$ states in HBr were recorded at room temperature and simulated. Band origins and

Fig. 5. Plots of $\ln(I(J)/S(3, \Omega', J))$ as a function of ground-state rotational energy ($E(J)$; $J = J''$) (see text) for various rotational line series (open circles, O; filled circles, P; open squares, Q; filled squares, R; open triangles, S; filled triangles, T) in the (3 + 1) REMPI spectrum of HBr due to the transition i($^3\Delta(2)$) $\leftarrow$X($^1\Sigma^+$), (0, 0). $I(J)$ are experimental intensities of rotational lines and $S(3, \Omega', J)$ are calculated absorption transition strengths. The continuous straight line is a best line fit through the experimental points. The broken line is for a thermal distribution corresponding to a room temperature (20°C). Plots (and curves) are normalized to fit straight lines with zero intersect values.

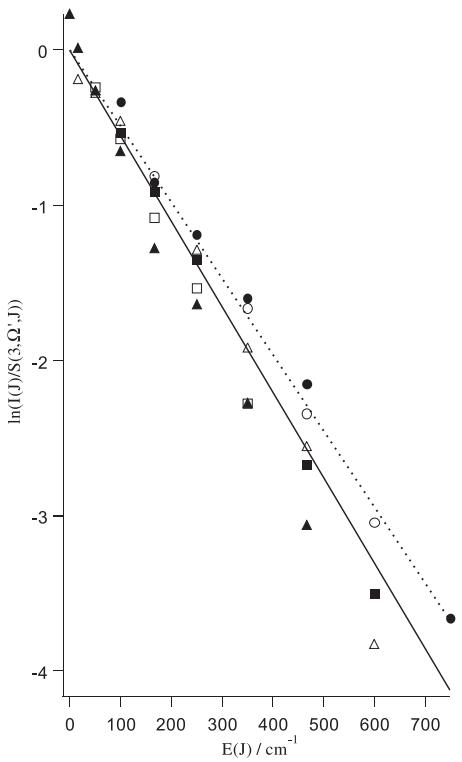

rotational constants for the excited state were derived from the simulation procedures. Good agreement is found between (2 + 1) and (3 + 1) REMPI spectra and with other researchers' data. Transition moment function parameters were evaluated from the (3 + 1) REMPI spectrum due to the E $\leftarrow$ X transition in HCl. These were interpreted in terms of the effect of intermediate states on the three-photon excitation mechanism. A (3 + 1) REMPI spectrum due to a $\Omega' = 3 \leftarrow \Omega'' = 0$ ($\Phi \leftarrow \Sigma$) transition at $\nu^o = 80\,167$ cm^{-1} was observed for the first time. Simulation of the spectrum allowed evaluations of spectroscopic constants for the newly observed state, which is assigned as the $l(^3\Phi(3))$ Rydberg state and the (0, 0) vibrational band. This state has the electronic configuration $(\sigma^2\pi^3)5d\delta$ and ion core term symbol $^2\Pi_{3/2}$. The expressions for the three-photon absorption strengths were used to derive rotational populations in the ground state from comparison of calculated and experimental (3 + 1) REMPI spectra due to the transition i($^3\Delta(2)$) $\leftarrow$X($^1\Sigma^+$) in HBr. The expressions are found to be useful for that purpose within experimental error.

Acknowledgment

The financial support of the University Research Fund, University of Iceland and the Icelandic Science Foundation is gratefully acknowledged. Furthermore, we are grateful for the inspiration given to us by Dr. Herzberg's work throughout the years.

References

1. C.R. Scheper, W.J. Buma, C.A. deLange, and W.J. v. d. Zande. J. Chem. Phys. **109**, 8319 (1998).
2. B.R. Lewis, S.T. Gibson, R.A. Copeland, and C.G. Bressler. Phys. Rev. Lett. **82**, 4212 (1999).
3. M. Wu and P.M. Johnson. J. Chem. Phys. **91**, 7399 (1989).
4. M.R. Dobber, W.J. Buma, and C.A. deLange. J. Chem. Phys. **101**, 9303 (1994).
5. C. Cossart-Magos, M. Jungen, and F. Launay. J. Chem. Phys. **109**, 6666 (1998).
6. C. Cossart-Magos, H. Lefebvre-Brion, M. Jungen, and F. Launay. J. Chem. Phys. **107**, 1308 (1997).
7. J.P. Berger, S. Couris, and D. Gauyacq. J. Chem. Phys. **107**, 8866 (1997).
8. B.G. Koenders, D.M. Wieringa, G.J. Kuik, K.E. Drabe, and C.A. deLange. Chem. Phys. **129**, 41 (1989).
9. Á. Kvaran, B.G. Waage, and H. Wang. J. Chem. Phys. **113**, 1755 (2000).
10. G. Herzberg. Molecular spectra and molecular structure; I. Spectra of diatomic molecules. 2nd ed. Van Nostrand Reinhold Co., New York. 1950.
11. R.G. Bray and R.M. Hochstrasser. Mol. Phys. **31**, 1199 (1976).
12. J.B. Halpern, H. Zacharias, and R. Wallenstein. J. Mol. Spectrosc. **79**, 1 (1980).
13. Y. Xie, P.T.A. Reilly, S. Chilukuri, and R.J. Gordon. J. Chem. Phys. **95**, 854 (1991).
14. S.J. Dixon-Warren, R.C. Jackson, J.C. Polanyi, H. Rieley, J.G. Shaper, and H. Weiss. J. Phys. Chem. **96**, 10 983 (1992).
15. R.C. Jackson, J.C. Polanyi, and P. Sjövall. J. Chem. Phys. **102**, 6308 (1995).
16. Á. Kvaran, Á. Logadóttir, and H. Wang. J. Chem. Phys. **109**, 5856 (1998).
17. Á. Kvaran, H. Wang, and Á. Logadóttir. J. Chem. Phys. **112**, 10 811 (2000).
18. D.S. Green, G.A. Bickel, and S.C. Wallace. J. Mol. Spectrosc. **150**, 303 (1991).
19. R. Callaghan and R.J. Gordon. J. Chem. Phys. **93**, 4624 (1990).
20. K.P. Hüber and G. Herzberg. Constants of diatomic molecules. Van Nostrand-Reinhold, New York. 1979.
21. Á. Kvaran, H. Wang, and Á. Logadóttir. *In* Recent research development in physical chemistry. Vol. 2. Transworld Research Network, India. 1998. pp. 233–244.
22. W. Huasheng, J. Ásgeirsson, Á. Kvaran, R.J. Donovan, R.V. Flood, K.P. Lawley, T. Ridley, and A.J. Yencha. J. Mol. Struct. **293**, 217 (1993).
23. Á. Kvaran, H. Wang, and J. Ásgeirsson. J. Mol. Spectrosc. **163**, 541 (1994).
24. T.E. Adams, R.J.S. Morrison, and E.R. Grant. Rev. Sci. Instrum. **51**, 141 (1980).
25. R.J. Donovan, A.C. Flexen, K.P. Lawley, and T. Ridley. Chem. Phys. **226**, 217 (1998).
26. A.E. Douglas and F.R. Greening. Can. J. Phys. **57**, 1650 (1979).
27. D.S. Ginter and M.L. Ginter. J. Mol. Spectrosc. **90**, 177 (1981).
28. D.S. Green, G.A. Bickel, and S.C. Wallace. J. Mol. Spectrosc. **150**, 388 (1991).
29. D.S. Ginter, M.L. Ginter, and S.G. Tilford. J. Mol. Spectrosc. **90**, 152 (1981).